Available online at www.sciencedirect.com
ScienceDirect
Control Engineering Practice 16 (2008) 685–696
CONTROL ENGINEERING PRACTICE
www.elsevier.com/locate/conengprac

An impact force compensation algorithm based on a piezo force sensor for wire bonding processes

Jung-Han Kim*, Chung-Hyuk Yim

School of Mechanical Design and Automation Engineering, Seoul National University of Technology, 172 Gongneung-dong, Nowon-ku, Seoul 139-743, South Korea

Received 26 August 2006; accepted 10 August 2007
Available online 25 September 2007

Abstract

Impact force control is a key factor in wire bonding processes affecting the overall quality of the product and productivity of the process. This paper presents an impact force compensation algorithm designed for gold wire bonding processes, which uses a piezo force sensor and contains a new algorithm design to reduce the impact force of the capillary when it contacts a silicon pad. This compensation algorithm was developed from an impedance model of the contact between the capillary and pad, and includes automatic drift cancellation calculations for the piezo force sensor. A flat-top impact force profile was achieved using this algorithm with the piezo force sensor attached to the *Z*-axis of the wire bonder. Tests were used to demonstrate that the proposed algorithm reduced the impact force dramatically, which is particularly important in fine pitch wire bonding processes.

Keywords: Impact control; Piezo force sensor; Contact detection; Force control; Wire bonding; Fine pitch

1. Introduction

The market trends of small consumer electronics such as cellular phones are very aggressive in the miniaturization of electronic packages. Ongoing demand for higher density and productivity of semiconductor packages is the main driving force for the development of precision assembly technologies in semiconductor processes. Recent trends in semiconductor assembly houses require 45-μm pad pitch wire bonding processes in the production line. Smaller pad sizes and finer pitches require various new techniques, such as micron-level control of the *xyz* system, more accurate current control of electronic flame-off devices, and especially impact moment control when the capillary tool tip contacts the pad or lead (Rooney, Nager, Geiger, & Shanguan, 2005).

Fig. 1 shows a 45-μm fine pitch gold wire bonding process. Gold wire bonding processes are thermosonic, which means that heat, ultrasonic energy, force, and time play important roles in the manufacturing process. The quality of the wire bonding is dependent on many subprocesses and material variables, such as the ultrasonic power, applied force, welding time, bond pad surface hardness, and interface temperature (Ding, Kim, & Tong, 2006).

Fig. 2 describes the movement of the capillary when it contacts a silicon pad. As the pad pitch decreases, the size of the free air ball (FAB) must also decrease, which degrades the ability to absorb an impact force. There are three major reasons why the impact force on the pad should be reduced to improve the quality of fine pitch wire bonding.

First, the impact force is directly related with the squashed ball size in the wire bonding process. If the impact force is too strong, the squashed ball becomes larger than the size of the pad, leading to a connection failure. In addition, it will not have proper bonding characteristics.

Second, a reduction in the impact force will increase the productivity of the entire wire bonding process by increasing the search speed. The search speed of the capillary must be much slower than that of a normal-sized pad in fine pitch wire bonding to reduce the impact force from the inertia of the *Z*-axis. A slow search speed for contact greatly increases the search time required for the contact. For example, a 10-mm/s search speed in an 80-μm search level will require approximately 8 ms for contact

*Corresponding author. Tel.: +82 2 970 6397; fax: +82 2 974 8270.
E-mail address: hankim@snut.ac.kr (J.-H. Kim).

0967-0661/$ - see front matter © 2007 Elsevier Ltd. All rights reserved.
doi:10.1016/j.conengprac.2007.08.002

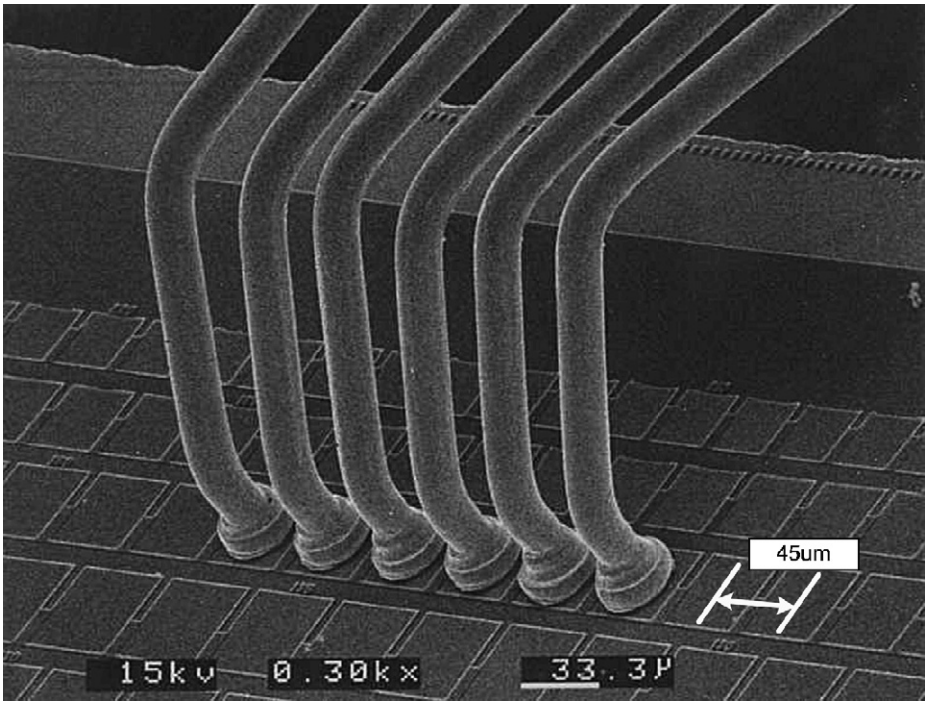

Fig. 1. A 45-μm pad pitch gold wire bonding process.

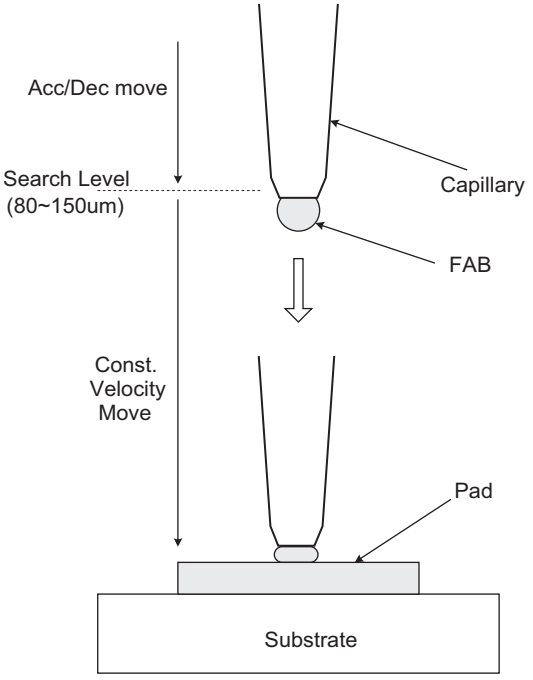

Fig. 2. Capillary with FAB contacts on the pad.

searching. However, if the speed must be decreased to 5 mm/s to reduce the impact force in the fine pitch case, the searching time will double to 16 ms for each contact. Chips usually have hundreds of pins and therefore their production units per hour (UPH) will be greatly affected by the search speed. The cost–time effectiveness is one of the most important issues in semiconductor manufacturing systems (Zafra-Cabeza, Ridao, Camacho, Kempf, & Rivera, 2007).

Third, the bonding quality will improve if the impact force is reduced. If the impact force is too great, the size of the squashed ball will instantly become too large and the ultrasonic generator (USG) will not be able to ensure an adequate amount of time to produce the intermetallic layer of the bonding surface. In addition, all bonding processes should have certain margins in their parameters for control of the mass production lines.

The measurement of the impact force exerted on a capillary tip during bonding is not an easy task because of the sensor location and various vibration noises. The location of the piezo sensor and electrode pattern greatly affects its sensitivity and measuring frequency (Chiu, Chan, Or, Cheung, & Liu, 2003). Recently, a special double beam force sensor was designed to provide force feedback in wire bonding processes (Yin, Zhou, Chen, Hu, & Lin, 2006).

Control of the impact force between two objects has been extensively researched in robotic control problems (Yoshikawa, 2000). In robotic application, usually both position control and force feedback are required for a given task. The main approaches for this type of problem are hybrid force control and impedance control. In the hybrid control strategy, a combination of motion control along one subspace and force control along another subspace is used (Raibert & Craig, 1981). Yoshikawa proposed a dynamic hybrid approach (Yoshikawa, 1987), and a nonlinear coordinate transform method was developed by McClamroch and Wang (1988). In the impedance force control strategy, it does not use both motion and force trajectories; rather, it controls the motion and force using the relationship between interactive forces and the position of the manipulator (Hogan, 1985).

There are several differences between robotic applications and compensating the impact force in wire bonding processes. In wire bonding, the capillary descends to the pad in a velocity control mode. After surface contact, the control mode of the *Z-axis* is immediately changed to a force control mode for the USG operation. The impact force is exerted over a very short instant, from 0.5 to 3 ms, between the velocity control mode and the force control mode. Therefore, a very fast response time is required to sense and compensate for the impact force in the transient area.

In this paper, a small stacked piezo force sensor was designed for the *Z*-axis of wire bonder, and an impact force compensation algorithm was newly developed based on an impedance model of the contact between the capillary and the pad. The following sections describe the design and implementation of the impact force compensation system and how the sensor drift problems were resolved. The experimental results showed that an ideal flat-top impact force profile could be achieved using the proposed compensation algorithm.

2. Design of the piezo force sensor for the *Z*-axis

A small piezo force sensor was designed to measure the impact force. The stacked piezo plates were electronically connected in parallel and attached to the *Z*-axis. Fig. 3 shows the piezo force sensor and the charge amplifier.

The piezo sensor responds to a change in strain. Piezo current i_{cr} is proportional to the strain change per unit time, and C_p, R_p in Fig. 3 are equivalent capacitance and resistance of piezo sensor, respectively (Doebrin, 1990). The output of the charge amplifier was adjusted to improve the low-frequency characteristics (Takaoka, Sakaguchi, Morita, Yamada, & Yamaguchi, 1997) and the output signal was digitized using a 16-bit A/D converter at a 16 kHz sampling frequency from a DSP board.

The *Z*-axis of a wire bonder executes various functions during the bonding process. The piezo force sensor attached to the *Z*-axis can be used for three purposes: it can measure the contact impact force, it can provide the USG profile feedback, and it can be used to control the force after contact while the USG is turned on. The location of the piezo force sensor can vary depending on its purpose. Chu, Chong, Chan, Ng, and Liu (2003) studied the effect of various sensor locations. The present research focuses on compensating and analyzing the first impact force. Fig. 4 shows the location of the sensor on the *Z*-axis between the transducer horn holder and the *Z*-axis body frame. When the tip of the *Z*-axis contacts a pad, the impact force is transmitted to the piezo sensor by the force

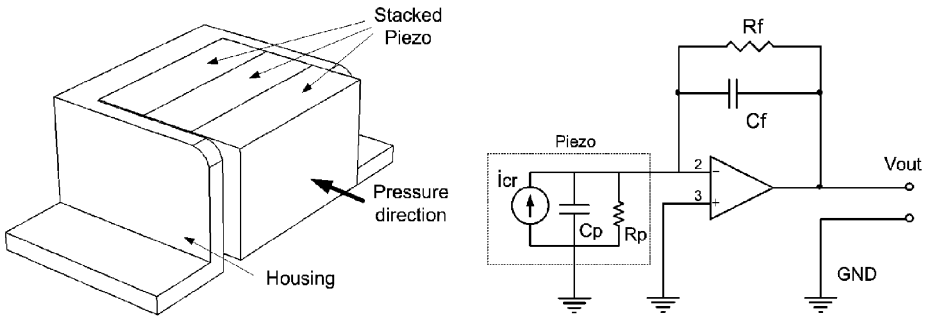

Fig. 3. Designed piezo force sensor and charge amplifier.

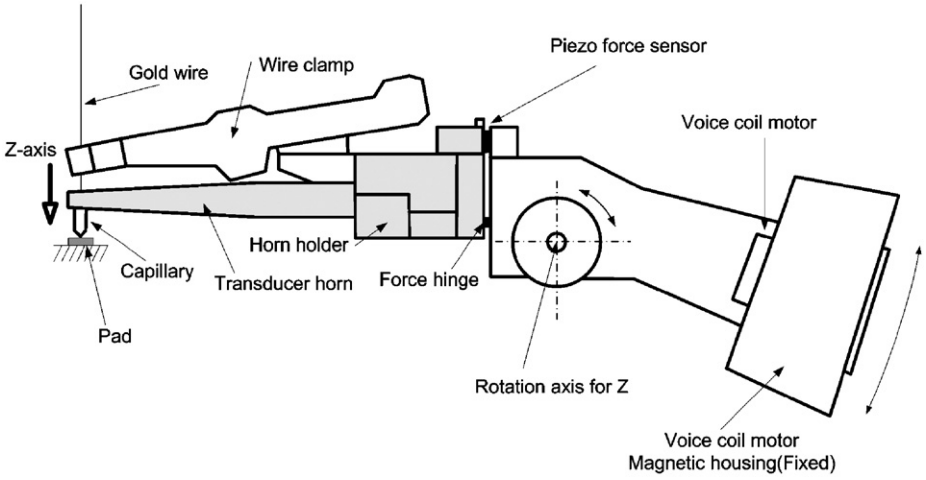

Fig. 4. Sensor location on the *Z*-axis of a wire bonder.

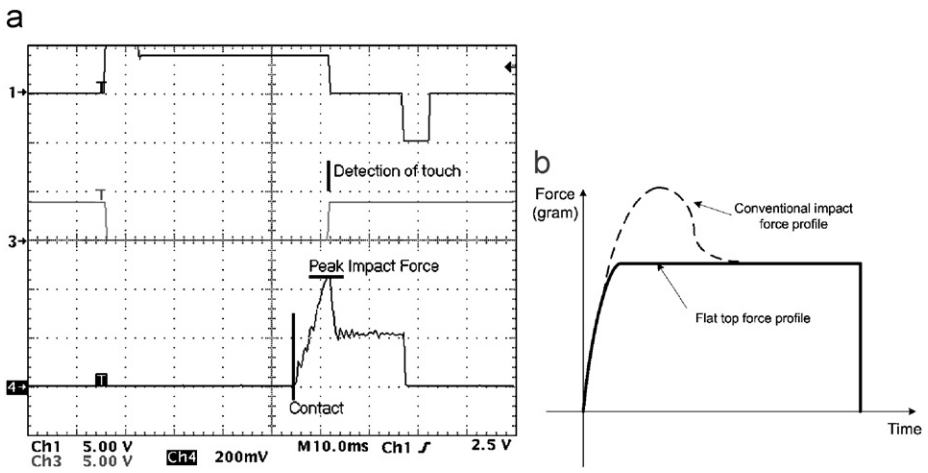

Fig. 5. The contact force profiles: (a) impact force measured by an external load cell (10 mm/s search speed) and (b) ideal flat-top impact force profile.

hinge. Due to the complex structure of the Z-axis, the alternative sensor locations are very limited. The final gain setting of the force sensor was approximately 30 mV/g f.

During the first bonding on a pad, the capillary descends at a constant speed until the surface contact is recognized. Fig. 5(a) shows the force profile (Channel 4) at the capillary contact point measured by an external load cell (Kyowa, DS-123). The impact force exerted by the capillary rises until the peak value is reached, which is directly proportional to the search velocity and the inertia of the Z-axis. Fig. 5(b) shows the ideal impact force profile, which has a flat top (Ding et al., 2006). The flat-top force profile has many advantages for controlling the characteristics of wire bonding, as described in Section 1.

3. Automatic drift cancellation and cascade digital filter

The piezo force sensor was designed to be attached between the horn holder and the Z-axis frame. Thus, it will respond to all Z-axis motions as well as the impact force. A new wire bonder has more than $120G$ of acceleration/deceleration in the Z-axis direction. This will excite all the mechanical structural parts, including the body, transducer horn, wire clamp, and force sensor supports. Therefore, the amplifier output also includes a large amount of noise from several mechanical vibration modes and the electrical encoder subdividing circuit (Zimmerman, Oshman, & Brandes, 2006).

After closely checking the resonance frequencies, three second-order IIR digital notch filters were designed and cascaded to reject the noise. One of the digital notch filters removes the first mode (1.1 kHz) of the horn resonance frequencies and can be described by

$$\frac{y_k}{x_k} = \frac{0.9638 - 1.7433z^{-1} + 0.9558z^{-2}}{1 - 1.7433z^{-1} + 0.9196z^{-2}}. \quad (1)$$

Fig. 6 shows the raw force sensor signal, the force sensor signal filtered by the cascaded notch filters, and the impact force signal measured by an external load cell to evaluate when the Z-axis is in a bonding cycle.

The piezo force sensor with a charge amplifier requires a low-frequency compensation function. A DC offset (at a very low frequency), however, always occurs in the signal, as shown in Fig. 6. The DC offset changes often and drifts with changes in temperature and acceleration (as the horn declines, the force sensor generates a DC offset). The best way to eliminate this drift is to measure it in the constant velocity area before tool contact and compensate for it at each bond. In this study, automatic drift cancellation calculations were performed using moving average (MA) filters.

The automatic drift cancellation was composed of three major signal processing blocks: a MA filter with a window size of 16 samples to provide low-frequency filtering of the sensor output, an MA filter with a window size of 32 samples to extract the drift offset quantity, and a drift capture timing signal generator. The drift capture timing signal was designed as follows. First, the total time to contact was calculated in advance. For example, a search level of 200 μm and a search velocity of 10 mm/s has a nominal time to contact of 20 ms. Second, the drift capture timing signal was calculated by multiplying by a timing factor. For example, a timing factor of 0.6 gives a drift capture time of 12 ms after the search level. This means that the output of the 32-samples MA filter will be captured 12 ms after the Z-axis passes the search level to measure the DC drift. This value will be subtracted from the output of the 16MA filter. Fig. 7 illustrates the measurement of force sensor DC drift and Fig. 8 gives a block diagram of the automatic drift cancellation.

The summarization of the algorithm is as follows. First, the cascaded notch filters filter out several bands of high frequencies; second, the 32MA filter extracts low-frequency drift component; finally, after a few milliseconds (for example, 12 ms) from the search level, the drift component is measured, and it is subtracted from the output of the 16MA filter.

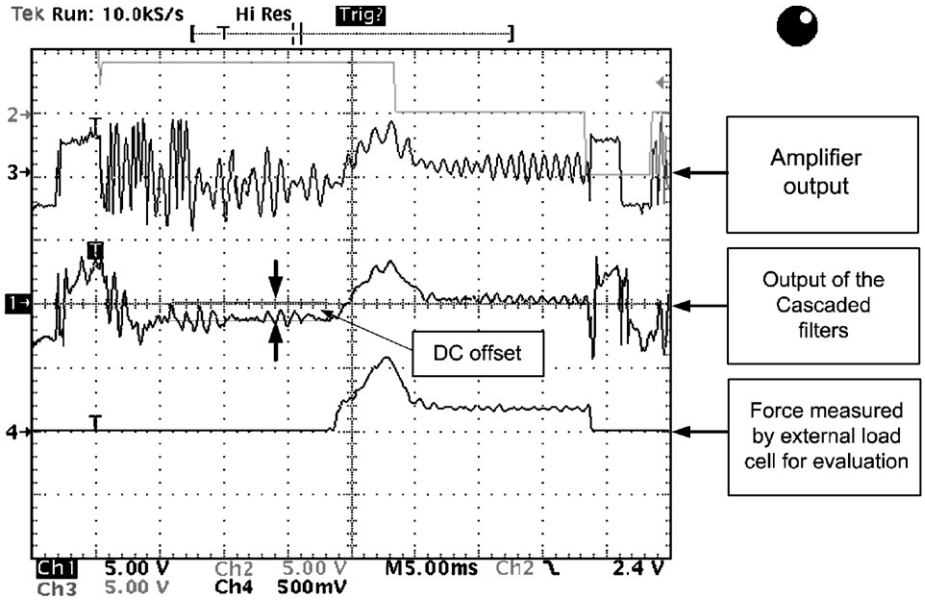

Fig. 6. Raw and filtered signals of the piezo force sensor (pad side bonding).

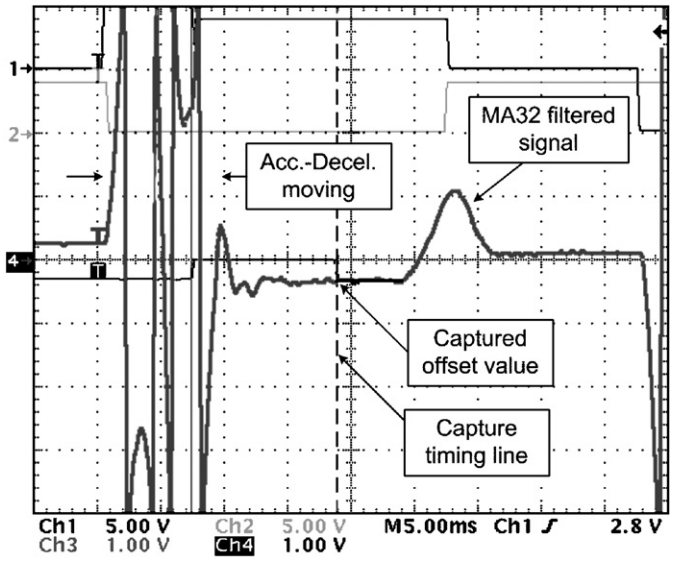

Fig. 7. Capturing the DC drift of a piezo force sensor.

4. Design of the impact force compensation algorithm

Fig. 9 shows the contact of a capillary with a FAB during the first bonding on a silicon pad. Here, z_c is the position where the FAB starts to contact and z_d is the desired position (squashed ball height).

The system shown in Fig. 9 can be modeled as

$$\tau = M_z\ddot{z} + C\dot{z} + K_e(z - z_c), \tag{2}$$

where τ is the motor force, M_z is the moving mass of the Z-axis, and C and K_e are the damping coefficient and FAB stiffness, respectively. The form of the governing Eq. (2) motivates the PD control law for the system stiffness (Yoshikawa, 1987). In this study, a reflective force control law was proposed:

$$\tau = K_{FP}(z_d - z) - K_{FV}\dot{z} + K_R(F_d - F_s), \tag{3}$$

where K_R, F_D, and F_s are the reflective force control gain, desired steady-state force (bonding force), and the output of the piezo force sensor, respectively, and K_{FP} and K_{FV} are positive scalar control gains. The closed loop system dynamics can be obtained by substituting Eq. (3) into Eq. (2):

$$M_z\ddot{z} + (C + K_{FV})\dot{z} + (K_e + K_{FP})z = K_e z_c + K_{FP}z_d + K_R(F_d - F_s), \tag{4}$$

which can be described by the block diagram given in Fig. 10.

If the three inputs of the block diagram in Fig. 10 are assumed stable, the closed loop system is also stable since the poles of the characteristic equation are in the open left-half s-plane. A Laplace transform of Eq. (4) is used to investigate the steady-state characteristics of the system:

$$Z(s) = \frac{K_e z_c + K_{FP}z_d + K_R(F_d - F_s)}{s(M_z s^2 + (C + K_{FV})s + (K_e + K_{FP}))}, \tag{5}$$

where the sensor output F_s is considered as constant in steady state. Therefore, the steady-state position of the Z-axis is

$$z_{ss} = \lim_{s\to 0} s\frac{K_e z_c + K_{FP}z_d + K_R(F_d - F_s)}{s(M_z s^2 + (C + K_{FV})s + (K_e + K_{FP}))} = \frac{K_e z_c + K_{FP}z_d + K_R(F_d - F_s)}{K_e + K_{FP}}. \tag{6}$$

Considering the model shown in Fig. 10, the steady-state force exerted on the pad can be modeled by

$$f_{ss} = K_e(z_{ss} - z_c). \tag{7}$$

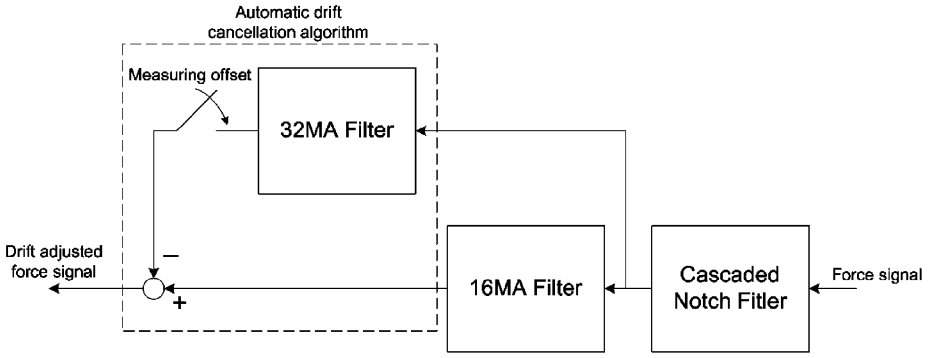

Fig. 8. Block diagram of the automatic drift cancellation.

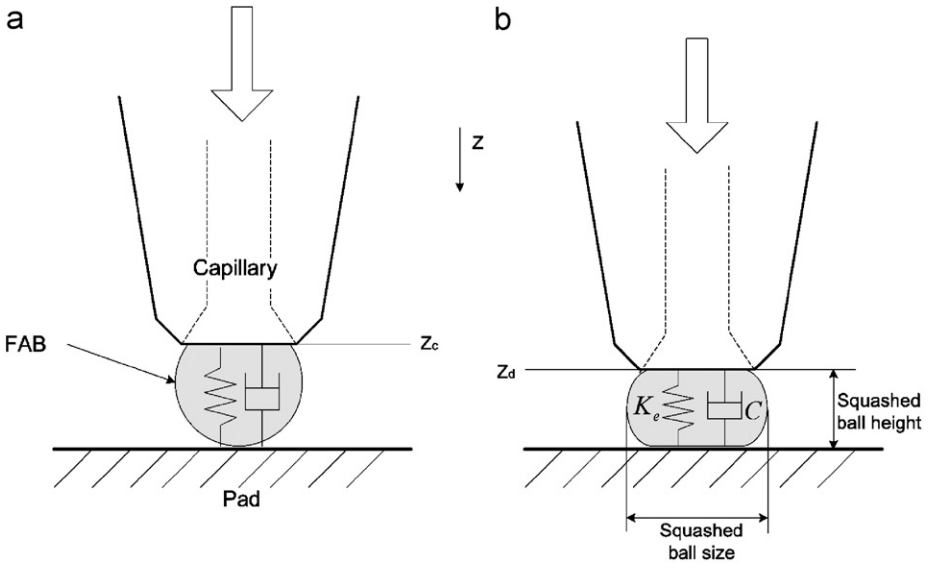

Fig. 9. Contact of the capillary with a FAB: (a) start of the capillary contact and (b) formation of the squashed ball.

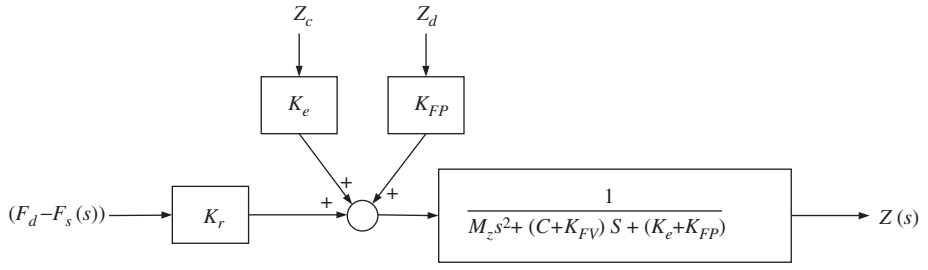

Fig. 10. Block diagram of the impact force compensation algorithm.

The steady-state force can be calculated by inserting Eq. (6) into Eq. (7):

$$f_{ss} = \frac{K_e K_{FP}(z_d - z_c) + K_e K_R (F_d - F_s)}{K_e + K_{FP}}. \tag{8}$$

If the amplitude of the piezo force sensor is tuned to the same scale ($f_{ss} = F_s$), Eq. (8) becomes

$$f_{ss} = \frac{K_e K_{FP}(z_d - z_c) + K_e K_R F_d}{K_e + K_{FP} + K_e K_R}. \tag{9}$$

The desired position (squashed ball height) can be defined as

$$z_d \equiv z_c + \alpha. \tag{10}$$

α means the z-axis position difference between the start of contact and the final position that is related with the squashed ball height. Then, the steady-state force of Eq. (9) will be

$$f_{ss} = \frac{K_e K_{FP}\alpha + K_e K_R F_d}{K_e + K_{FP} + K_e K_R}. \tag{11}$$

If the FAB stiffness K_e and the control gain K_{FP} are sufficiently small compared to the reflective force gain K_R (K_e, $K_{FP} \ll K_R$), the steady-state force f_{ss} will be similar to the desired bonding force F_d:

$$f_{ss} \approx F_d. \tag{12}$$

It is not an easy task to calculate the FAB stiffness coefficient K_e. Therefore, the control gains K_{FP}, K_{FV}, and K_R in Eq. (3) must be tuned by trial and error to obtain the flat-top force profile shown in Fig. 5(b).

5. Block diagram of the system structure

The sequential signal flow of the impact force compensation algorithm is composed of three phases: the digital filtering of unimportant frequencies by the cascaded digital notch filters, the measurement and compensation of the DC drift, and the control of the impact force. Fig. 11 shows an overall block diagram of the impact force compensation algorithm.

The peak impact force of Fig. 5(a) usually occurs before the contact is detected. Therefore, the impact force compensation algorithm must run independently of the contact detection algorithm (Kim & Park, 2006). The output of the impact force compensation algorithm is added directly to the torque output of the velocity controller. Owing to this independent structure from the detection algorithm, excess pushing force can be effectively eliminated without time lag. The output of the impact force compensator has a threshold value to prevent the Z-axis from crushing due to an abnormal sensor output. Fig. 12 shows the signal flow between the algorithm and the DAC output.

The On/Off Control box in Fig. 12 is designed for the algorithm to run only in the search–impact period (between search level and impact position of the z-axis). This software switch prevents the velocity control loop from being disturbed by the output of the algorithm when the Z-axis is in other modes.

6. Experimental results

The proposed impact force compensation algorithm, including the automatic drift cancellation algorithm, was fully tested and verified with test equipment and on a test machine in a manufacturing line. Fig. 13 shows the

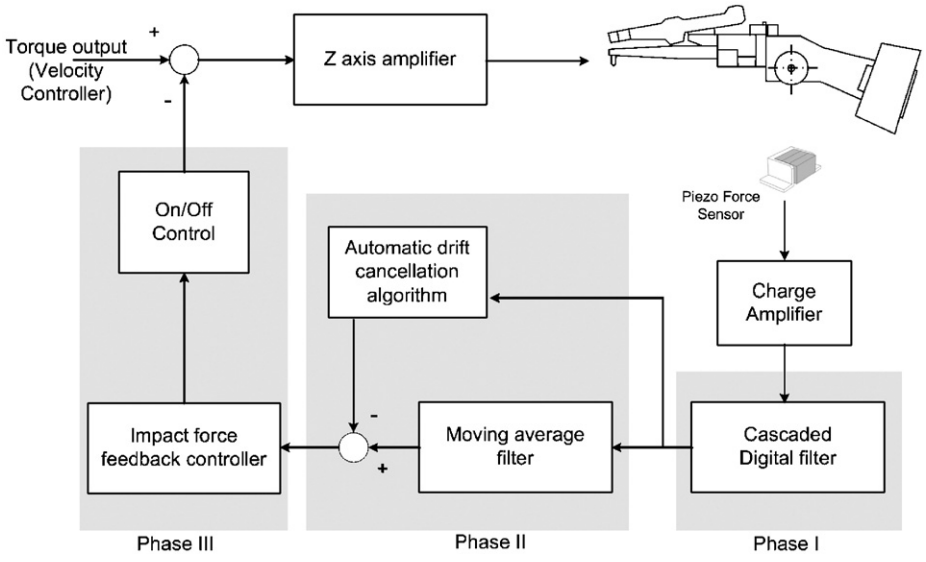

Fig. 11. Overall block diagram of the impact force compensation algorithm.

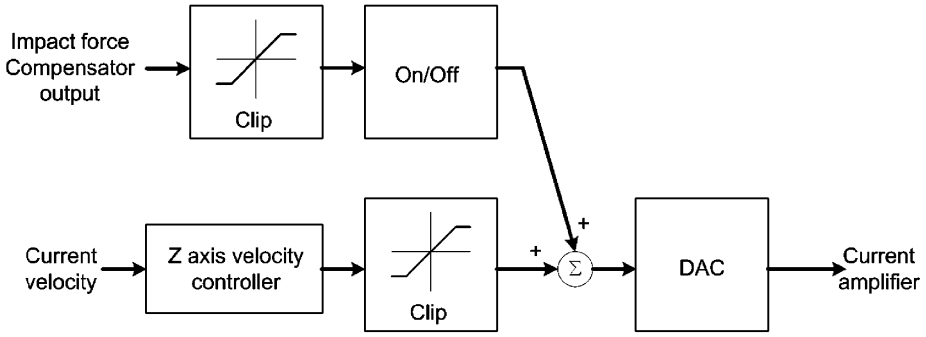

Fig. 12. Signal flow between the algorithm and the DAC output.

test equipment. A special jig with a miniature load cell (LM-1KA, Kyowa) and an instrumental amplifier were used to evaluate the algorithm. The jig had the same dimensions as the heater block on the front rail of the wire bonder so that the external load cell could be easily set to the exact spot of the capillary contact. The external load cell was used only to evaluate the impact force compensation system.

Figs. 14–19 (channel 4) shows the impact force profiles that were measured by the external load cell for search velocities varying from 25 to 3 mm/s. Each figure shows the results with the proposed algorithm turned on and off. The bond force in all cases was set to 20 gf, and the bonding time was 15 ms. The figures clearly indicate that the peak impact forces were reduced considerably by the proposed algorithm, especially when the search velocity was 5 mm/s

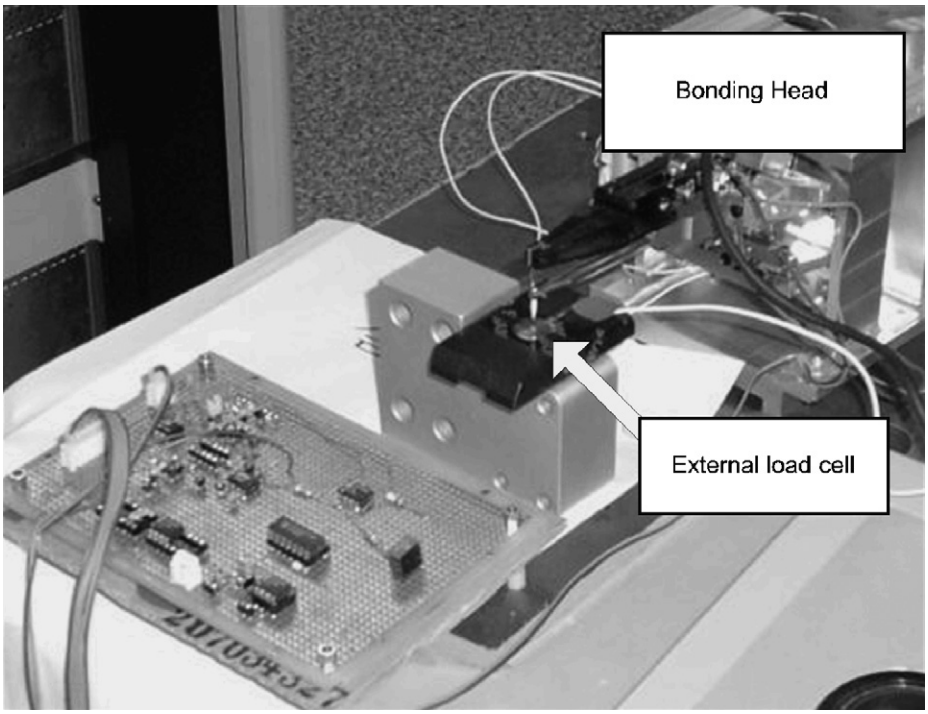

Fig. 13. Test equipment with an external load cell.

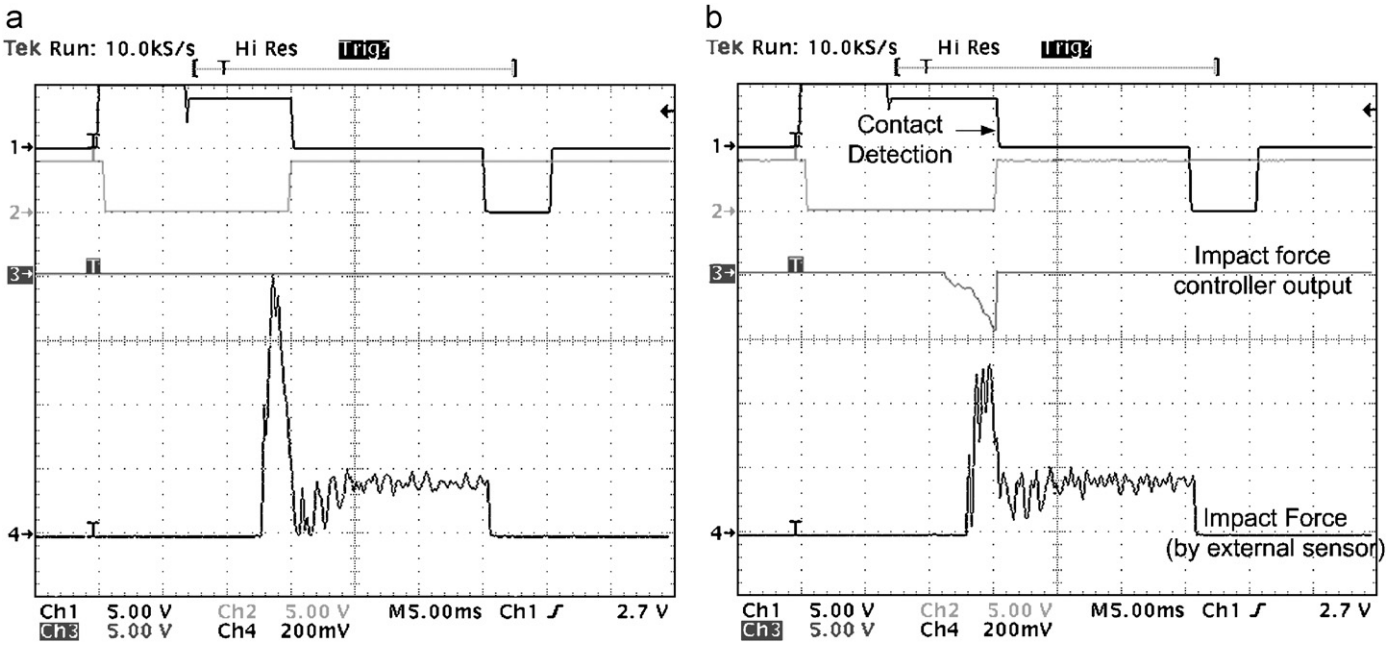

Fig. 14. Impact force profile (channel 4, search velocity is 25 mm/s), (a) impact force compensation off and (b) impact force compensation on.

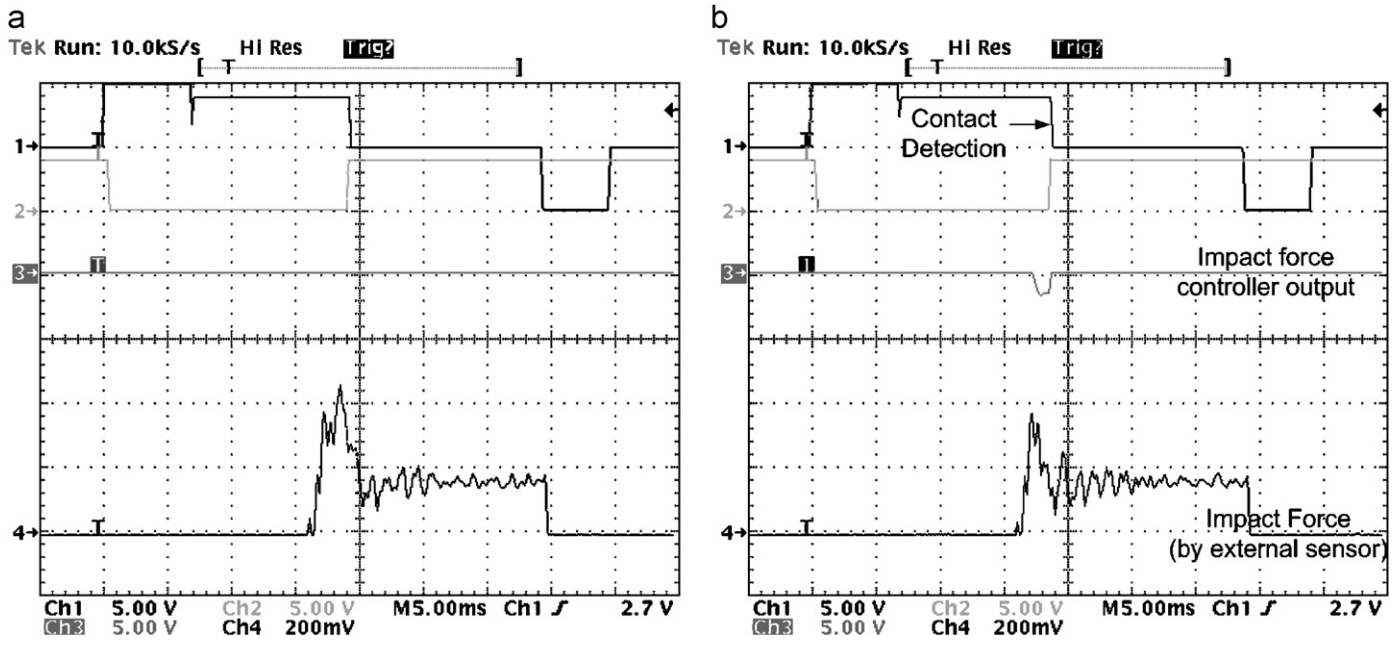

Fig. 15. Impact force profile (channel 4, search velocity is 15 mm/s), (a) impact force compensation off and (b) impact force compensation on.

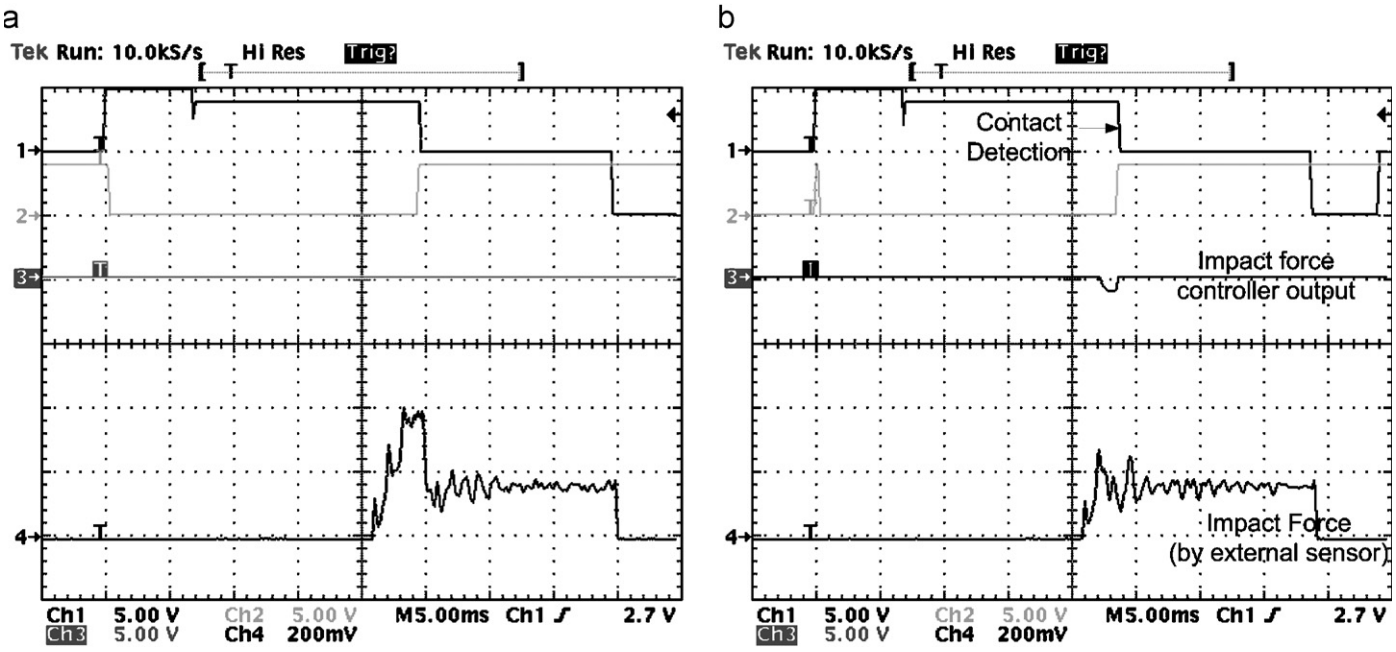

Fig. 16. Impact force profile (channel 4, search velocity is 10 mm/s), (a) impact force compensation off and (b) impact force compensation on.

(Fig. 18) and 3 mm/s (Fig. 19), which are the most frequently used search velocities in fine pitch processes. Flat-top impact force characteristics were also achieved, which improves the lifetime of the capillary and increases the mean time between assists. The peak impact force was reduced from 100 to 65 gf when the search velocity was 25 mm/s (Fig. 14), which is a 35% reduction. Table 1 summarizes the average reduction of the peak impact force by the proposed algorithm. The values in Table 1 are averages of 20 tests for each search velocity. On average, the peak impact forces were decreased by 41%.

Impact force and search velocity has a relation which can be expressed as the following momentum equation:

$$Tt = Flt = I(\dot{\theta}_2 - \dot{\theta}_1), \tag{13}$$

where T, F, l, t, I are torque, impact force, moment arm (from capillary to the hinge), contact time, and rotational

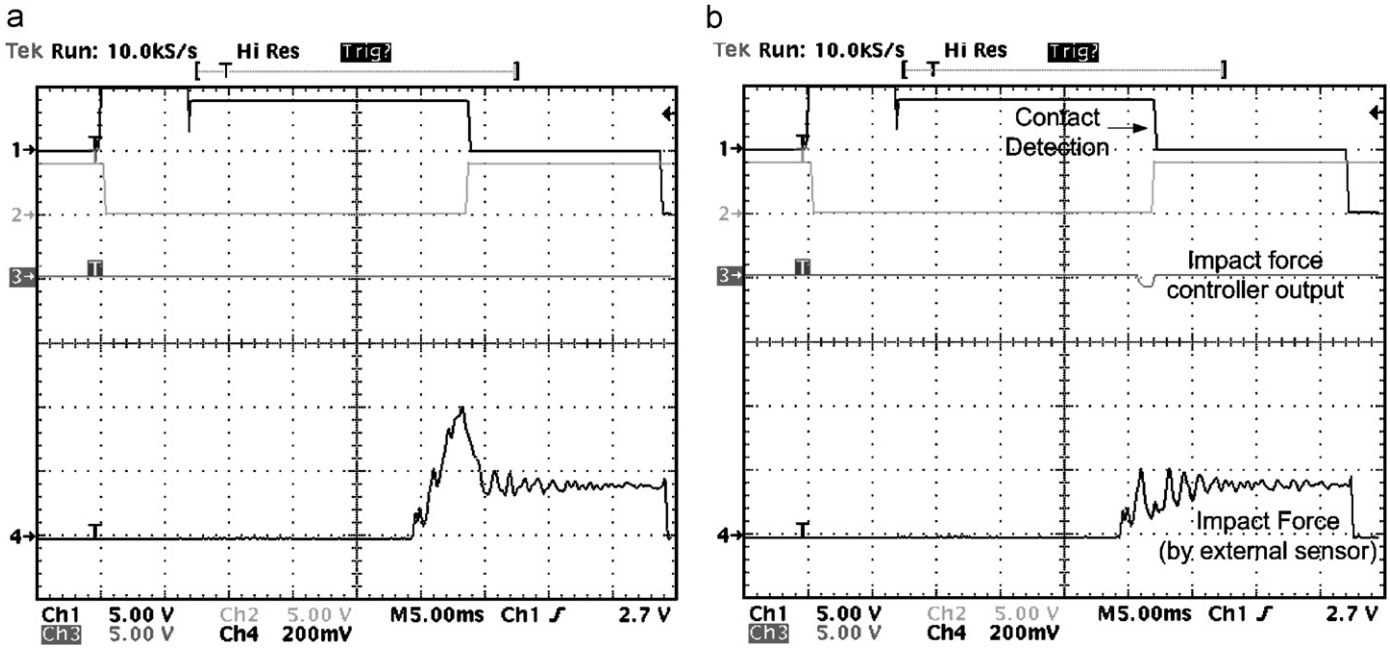

Fig. 17. Impact force profile (channel 4, search velocity is 8 mm/s), (a) impact force compensation off and (b) impact force compensation on.

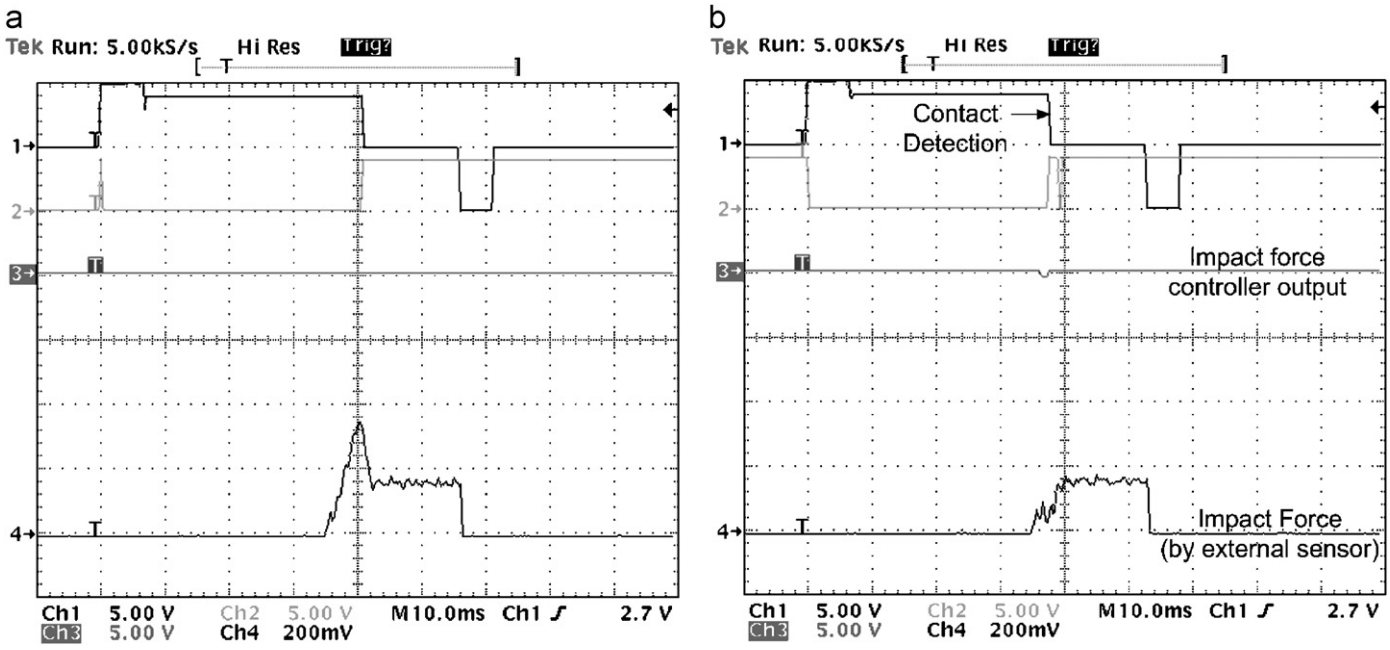

Fig. 18. Impact force profile (channel 4, search velocity is 5 mm/s), (a) impact force compensation off and (b) impact force compensation on.

inertial moment, respectively. $\dot{\theta}_n$ is a rotational speed at the hinge. After the impact, $\dot{\theta}_2$ can be assumed as zero, and the impact force (F) will be proportional to the search speed ($\dot{\theta}_1$) for the same contact time.

The force profiles shown in Figs. 14–19 were measured without a FAB because the capillary impact must be on the face of the external load cell. If a FAB were present on the capillary tool tip, it would increase the system damping coefficient, reducing the small amount of vibrations in the force profile after contact.

If the search velocity could be increased from 5 to 10 mm/s, it would increase the productivity of the wire bonding process and the UPH would be increased by 11% for the case of a chip with 208 pins. Table 2 lists the

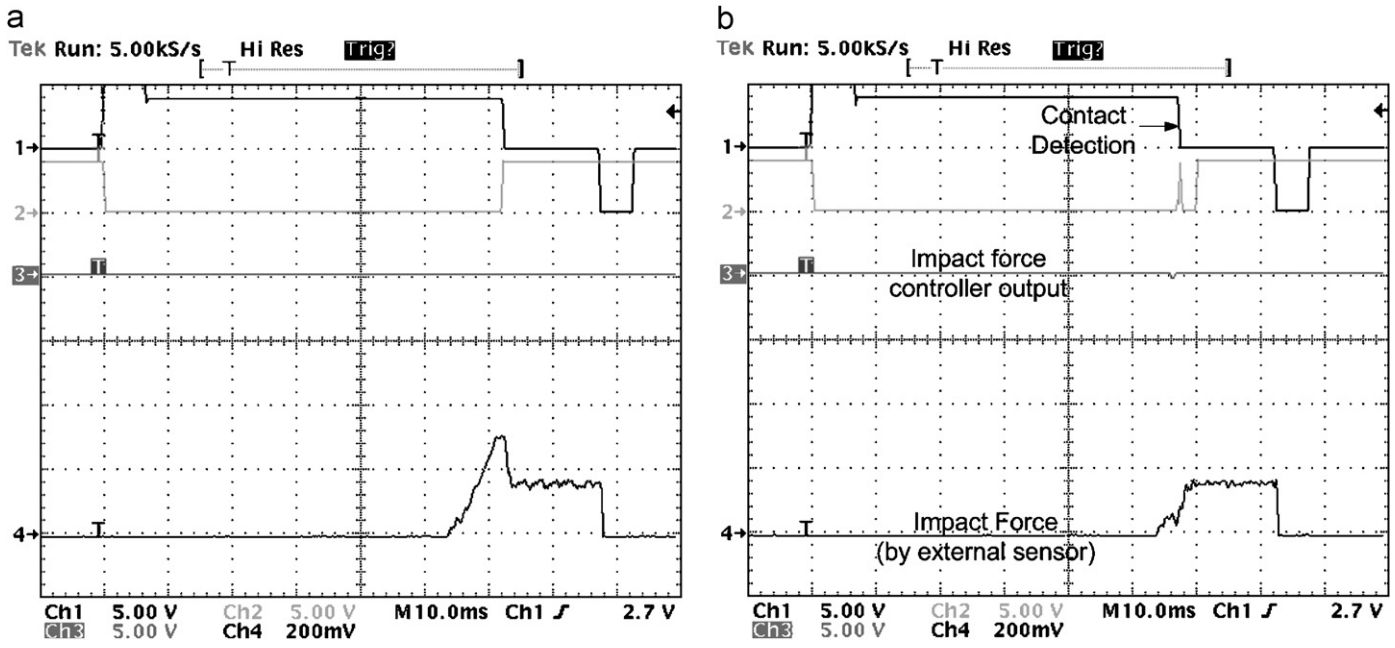

Fig. 19. Impact force profile (channel 4, search velocity is 3 mm/s), (a) impact force compensation off and (b) impact force compensation on.

Table 1
Peak impact force reduction

Search velocity (mm/s)	Impact force compensation off (gf)	Impact force compensation on (gf)	Peak force reduction ratio (%)
25	101	64	36
20	72	51	29
15	60	43	28
10	49	26	47
8	48	23	52
5	45	21	53
3	37	21	43
Average			41

Table 2
Expected productivity improvements with increases in search velocity (208 pins)

First bonding (pad)		Second bonding (lead)		1 wire bonding time (ms)	UPH (estimated)
Search height (μm)	Search velocity (mm/s)	Search height (μm)	Search velocity (mm/s)		
150	5	150	15	146.8	102.5
150	8	150	20	133.0	111.6
150	10	150	25	127.8	115.5
150	12	150	25	125.3	117.5
150	15	150	25	122.8	119.5

expected productivity improvements if the search velocities could be increased for the first bond (pad) and the second bond (lead).

7. Conclusions

Conventional efforts to reduce the impact force at a given contact speed have focused on reducing the inertia of the Z-axis. But as the movement specification of the Z-axis increases, it becomes more difficult to reduce the inertia of the moving part of the wire bonder head. The proposed impact force compensation algorithm reduced the peak impact force, allowing wider parameter USG margins (bonding force, bonding time, and heater temperature) and an improvement in productivity. Parameter margins are very important for controlling the quality of the mass production, and they allow the wire bonder to be adapted to various other types of work materials. A reduction of the impact force also benefits work materials that have flexible substrates.

Most semiconductor manufacturing machines, including wire bonders, run 24 h a day, and a small improvement in the productivity brings many benefits to the semiconductor manufacturer. An improvement in the UPH from the impact force compensation algorithm also strengthens the price competitive power of the product.

In this study, a contact model between an FAB and a pad was built, and an impact force compensating algorithm based on an impedance model was developed, including a drift compensation algorithm for a piezo force sensor. The drift compensation was designed using several notch and MA filters and digital signal processing. The experimental results showed that the ideal flat-top impact force profile was achieved using the proposed compensating algorithm, which improves the productivity of the wire bonding process.

References

Chiu, S. S., Chan, H. L. W., Or, S. W., Cheung, Y. M., & Liu, P. C. K. (2003). Effect of electrode pattern on the outputs of piezosensors for wire bonding process control. *Material Science and Engineering*, *B99*, 121–126.

Chu, P. W. P., Chong, C. P., Chan, H. L. W., Ng, K. M. W., & Liu, P. C. K. (2003). Placement of piezoelectric ceramics sensors in ultrasonic wire bonding transducers. *Microelectronics Engineering*, *66*, 750–759.

Ding, Y., Kim, J. K., & Tong, P. (2006). Effects of bonding force on contact pressure and frictional energy in wire bonding. *Microelectronics Reliability*, *46*, 1101–1112.

Doebrin, E. O. (1990). *Measurement systems—Application and design* (4th ed). Singapore: McGraw-Hill pp. 261–268.

Hogan, N. (1985). Impedance control: An approach to manipulation: Part I—Theory. *Journal of Dynamic systems, Measurement, and Control*, *107*, 1–7.

Kim, J. H., & Park, H. J. (2006). A contact detection algorithm of the *z*-axis of a wire bonder. *Control Engineering Practice*, *14*, 1035–1043.

McClamroch, N. H., & Wang, D. (1988). Feedback stabilization and tracking of constrained robots. *IEEE Transactions on Automatic Control*, *33*(5), 419–426.

Raibert, M. H., & Craig, J. J. (1981). Hybrid position/force control of manipulators. *Journal of Dynamic Systems, Measurement, and Control*, *102*, 126–133.

Rooney, D. T., Nager, D. P., Geiger, D., & Shanguan, D. (2005). Evaluation of wire bonding performance, process conditions, and metallurgical integrity of chip on board wire bonds. *Microelectronics Reliability*, *45*, 379–390.

Takaoka, D., Sakaguchi, A., Morita, Y., Yamada, M., & Yamaguchi, T. (1997). Piezoelectric mount force sensor of placement system for surface mount devices. *Journal of Japanese Precision Engineering*, *63*, 664–668.

Yin, Y., Zhou, C., Chen, S., Hu, H., & Lin, Z. (2006). Optimal design of micro-force sensor for wire bonding with high acceleration and frequency movement. *Sensors and Actuators A*, *127*, 104–118.

Yoshikawa, T. (1987). Dynamic hybrid position/force control of robot manipulator: Description of hand constraint and calculation of joint driving force. *IEEE Journal of Robotics and Automation*, *3*(5), 386–392.

Yoshikawa, T. (2000). Force control of robot manipulators. In: *Proceedings of the IEEE conference on robotics and automation*, San Francisco (Invited Session) (pp. 220–226).

Zafra-Cabeza, A., Ridao, M. A., Camacho, E. F., Kempf, K. G., & Rivera, D. E. (2007). Managing risk in semiconductor manufacturing: A stochastic predictive control approach. *Control Engineering Practice*, *15*, 969–984.

Zimmerman, Y., Oshman, Y., & Brandes, A. (2006). Improving the accuracy of analog encoders via Kalman filtering. *Control Engineering Practice*, *14*, 337–350.